https://doi.org/10.5194/egusphere-2026-1808
Preprint. Discussion started: 10 April 2026

Physical transport processes in the fjords of South Georgia

Annika Oetjens[1,2,3], Wilken-Jon von Appen[1], Joséphine Anselin[4,5], Berenice Ebner[1,6], Florian Koch[1], Kai-Uwe Ludwichowski[1], Ryan Mole[1], Joanna Zanker[4], Emma Young[4], and Sabine Kasten[1,6,7]

[1]Alfred Wegener Institute Helmholtz Centre for Polar and Marine Research, Bremerhaven, Germany
[2]Institute for Marine and Antarctic Studies (IMAS), University of Tasmania, Hobart, Australia.
[3]Australian Centre for Excellence in Antarctic Science (ACEAS), University of Tasmania, Hobart, Australia.
[4]British Antarctic Survey, Cambridge, UK
[5]Department of Applied Mathematics and Theoretical Physics, University of Cambridge, Cambridge, UK
[6]University of Bremen, Faculty of Geosciences, Klagenfurter Straße 2-4, 28359 Bremen, Germany
[7]MARUM- Center for Marine Environmental Sciences, University of Bremen, Leobener Str. 8, 28359 Bremen, Germany

Correspondence: Annika Oetjens (Annika.Oetjens@utas.edu.au)

Abstract. The Southern Ocean, typically characterized as a high-nutrient, low-chlorophyll region, exhibits recurring chlorophyll blooms downstream of South Georgia island fuelled by iron enrichment of near-surface water. To better understand the physical processes underpinning iron and nutrient transport from South Georgia fjords to the surrounding shelf, extensive data were collected during research cruise PS133.2 of RV *Polarstern* in late austral spring 2022. Here, we present analyses of these data to characterize water masses, circulation patterns and nutrient distribution inside Cumberland Bay East and King Haakon Bay including the adjacent shelf. Surface currents are influenced by westerly winds, particularly on the eastern side of the island. Fjord-shelf exchange in Cumberland Bay East exhibit weak export and residence times are on the order of days to months driven by a vertical overturning circulation. The highest temperature and chlorophyll values are measured at the mouth of King Haakon Bay. The results highlight the diverse local environment and the significant influence of bathymetry and orography on fjord systems at South Georgia. This study elucidates the physical transport processes of fjord-shelf exchange that may support transport of iron and nutrients as a source for the downstream chlorophyll blooms in the open ocean. Ongoing investigations will further explore the biological and geochemical aspects, providing a comprehensive understanding of the South Georgia system.

https://doi.org/10.5194/egusphere-2026-1808
Preprint. Discussion started: 10 April 2026

1 Introduction

South Georgia (54.3° S, 36.5° W) is located in the Southern Ocean and has gained significant attention due to its unique marine ecosystem characterized by high productivity and biodiversity (e.g., Nielsdóttir et al., 2012; Korb and Whitehouse, 2004; Korb et al., 2008, 2005; Ward et al., 2007). The Southern Ocean surrounding South Georgia is known for its iron-limited conditions, which contribute to the high-nutrient, low-chlorophyll nature of the region (Martin, 1990). Satellite images have revealed a seasonal chlorophyll bloom downstream of the island. When iron is introduced into iron-limited areas it acts as a fertilizing agent and promotes the growth of phytoplankton (e.g., Coale et al., 1996; Behrenfeld et al., 1996; Martin et al., 1990). Phytoplankton are not only the basis of the marine food web but essential to the biological carbon pump, where carbon is transferred from the surface waters to the deep ocean as organic matter sinks (e.g., Boyd et al., 2019).

As part of the multi-disciplinary *Island Impact* study on-board RV *Polarstern* in late austral spring between 20th November and 19th December 2022, we investigate two of the fjord systems of the island to get an account of the sources and transport mechanisms enabling the yearly bloom. Here, we focus on the fjord dynamics in Cumberland Bay East (CBE) and King Haakon Bay (KHB) (Fig. 1).

1.1 The role of the Antarctic Circumpolar Current

The Antarctic Circumpolar Current (ACC) is the largest current system in the world, transporting on the order of 140 Sv of water in an eastward direction around Antarctica (Koenig et al., 2016). In the absence of zonal barriers the ACC connects the basins of the Atlantic, Pacific and Indian oceans, carrying tracers between them and around the globe. In addition to this horizontal transport, vertical transport in the ACC, which sees nutrient-rich, deep water drawn poleward toward the surface along steep-sloping isopycnals, forms a vital link in global meridional overturning (Orsi et al., 1995). Several strong jets appear along the density fronts associated with these sloping isopycnals and dominate the eastward flow. Some of the saline, nutrient-rich Circumpolar Deep Water which has risen along isopycnals outcrops to the surface near the southernmost front of the ACC and is transported northwards by Ekman transport in the surface layers where its nutrients are available for primary production. It is freshened and modified into Antarctic Surface Water as it travels before finally descending below warmer, saltier Atlantic surface waters at the Polar Front to form global intermediate waters. The Southern ACC Front lies between these two fronts and separates fresher Antarctic surface water to the north from those more recently in contact with deeper waters to the south. South Georgia island (Fig. 1) lies directly between the Polar Front and Southern ACC Front where the ACC takes a meridional diversion away from its usual zonal path to exit the Scotia Sea. The Polar Front finds a route through the North Scotia Ridge and passes South Georgia to the north through the South Georgia Basin. The Southern ACC Front interacts more strongly with South Georgia, flowing toward the south-western edge of the South Georgia shelf before wrapping around its southern edge (Matano et al., 2020). A portion of the waters carried in the Southern ACC Front flow westward into the South Georgia basin at a bifurcation once they reach the north-eastern side of the South Georgia shelf, with the rest continuing further downstream to the east. An other mechanism relevant for the open ocean is the wind-driven Ekman buoyancy flux supplying iron from below the mixed layer and supporting intense phytoplankton blooms (Mole et al., 2025).

https://doi.org/10.5194/egusphere-2026-1808
Preprint. Discussion started: 10 April 2026

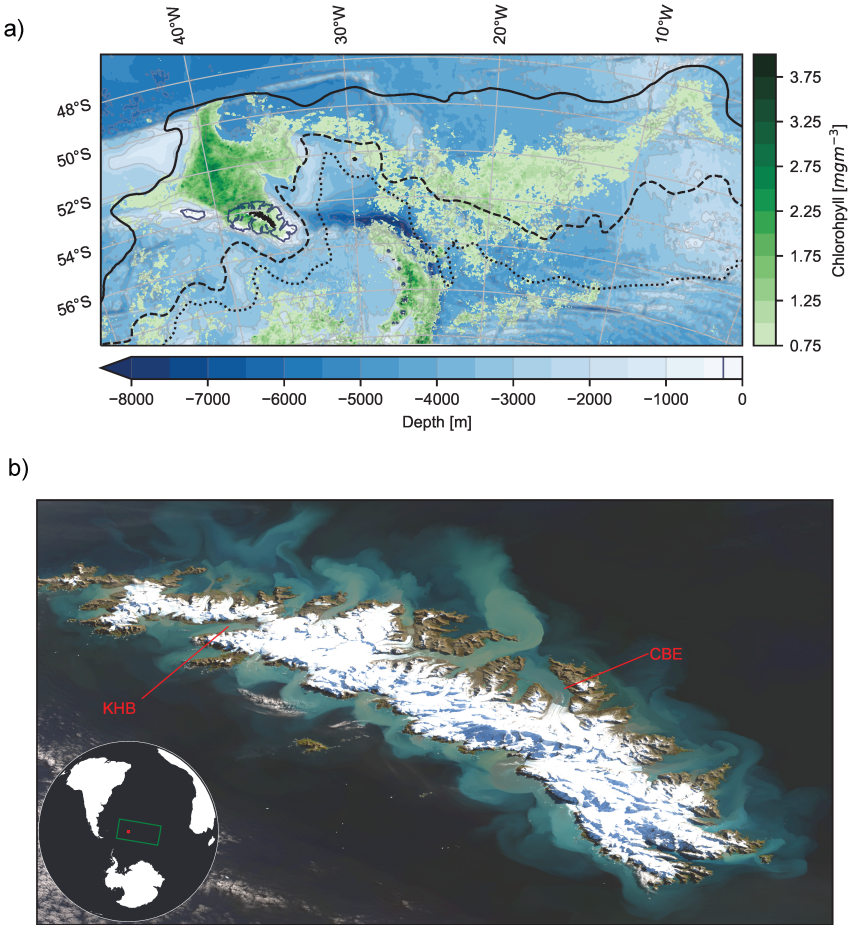

Figure 1. Overview of the study region with chlorophyll climatology (green shading) for January (2013-–2022, Copernicus Marine Service and PML (2022). Accessed on 21-07-2023), showing values above 0.75 mg m^{-3} only. GEBCO bathymetry (GEBCO Bathymetric Compilation Group 2023, 2023) (blue shading) with the 250 m contour defining the shelf edge (blue line). Major fronts of the Antarctic Circumpolar Current (ACC) are shown in black (solid: Polar Front, dashed: Southern ACC Front, dotted: Southern Boundary, (Park et al., 2019)). b) Satellite image of South Georgia with visible meltwater plumes spreading out from its fjords (Landsat-8 image courtesy of the U.S. Geological Survey, captured 28-03-2018). Cumberland Bay East (CBE) and King Haakon Bay (KHB) are indicated in red. Inset map shows the extent of panel a) with a green box and the location of South Georgia Island (red dot).

1.2 Island mass effect

The islands in the Southern Ocean play a significant role in natural iron fertilization, often referred to as the island mass effect, where the presence of islands enhances the availability of nutrients and iron in the surrounding waters, leading to increased primary productivity and biological activity (e.g., Robinson et al., 2016).

https://doi.org/10.5194/egusphere-2026-1808
Preprint. Discussion started: 10 April 2026

The island mass effect has been observed in various regions of the Southern Ocean, such as the Crozet Islands, Kerguelen Islands (in the Indian sector), and South Georgia (in the Atlantic sector) (Pollard et al., 2007; Blain et al., 2001). The CROZEX study (Pollard et al., 2007) confirmed that iron fertilized the annual bloom around the Crozet Islands where phytoplankton production rates are much larger than in the high-nutrient, low-chlorophyll control area (Bakker et al., 2007). On the Kerguelen plateau, the KEOPS and KEOPS-2 study (Blain et al., 2001) investigate another bloom initiated by natural iron fertilization. *Island Impact* complements these studies.

These sub-Antarctic islands support diverse ecosystems and contribute to increased primary productivity in their surrounding waters. They serve as hotspots of biological activity, attracting a range of marine organisms, including birds, seals, and whales, which rely on the increased availability of food (Borrione and Schlitzer, 2013; Young et al., 2012) .

Due to the island mass effect it can be assumed that the iron supply would be plentiful and the main driver of the observed increases in primary production the region of ocean surrounding South Georgia. This is a stark contrast to the iron-limited conditions in the wider Southern Ocean. The interaction between the availability of iron and other nutrients with the hydrography likely shapes the ecological processes in this area. Understanding the physical conditions, including the transport of water masses and nutrients, is crucial for understanding the nutrient exchange processes between the fjords and the adjacent continental shelf region and the resulting phytoplankton blooms. While previous observations and models have already provided valuable insights into the circulation patterns around the South Georgia shelf (Young et al., 2011; Meredith, 2003; Brandon et al., 1999), a detailed understanding of the drivers behind these dynamics is lacking.

Natural sources, such as upwelling of nutrient-rich waters and glacial meltwater runoff, are significant contributors to the iron supply in this area (Robinson et al., 2016; Raiswell et al., 2008). Upwelling events associated with the ACC transport nutrient-rich deep waters to the surface, potentially supplying iron to the euphotic zone. Furthermore, the island's unique geology and glacial history contribute to local sources of iron, including weathering processes and subglacial meltwater runoff (Borrione et al., 2014; Korb and Whitehouse, 2004; Nielsdóttir et al., 2012; Whitehouse et al., 1996). A modelling study of circulation within Cumberland Bay has demonstrated that circulation patterns in the island fjords can be complex (Zanker et al., 2024). Atmospheric dust deposition, carried by winds over long distances, can also deliver iron particles to the surface waters but Borrione et al. (2014) found these to be unimportant for the South Georgia bloom.

1.3 Glaciers and meltwater discharge

Melting glaciers and the resulting increased meltwater discharge can stimulate the release of nutrients (e.g., Fe, Si, N, P), which are ultimately transported either via sediment-laden meltwater plumes or via icebergs to the ocean (Borrione et al., 2014; Raiswell et al., 2008; Wadham et al., 2013). Nutrient and iron fluxes may change under global warming and not all the potential iron sources (e.g. weathering, erosion, glacial meltwater, submarine groundwater discharge, benthic fluxes, sea-ice melt) are expected to respond equally to climate change. Glaciers in South Georgia overlay bedrock lithologies that vary across the island and consequently supply differing quantities of trace metals to the ocean via physical weathering processes at the ice-bed interface (Wadham et al., 2013). The CBE and KHB fjord systems are outlets for large tidewater glaciers, including Nordenskjöld, Hamberg, Harker and Briggs Glacier. CBE is 15 km long and 3–5 km wide, with an average depth of ∼200 m.

https://doi.org/10.5194/egusphere-2026-1808
Preprint. Discussion started: 10 April 2026

Nordenskjöld Glacier is the largest marine terminating glacier in CBE, assumed to have a grounded, roughly vertical calving front where mass is lost through a combination of submarine melting, likely enhanced by subglacial plumes, and calving (Hodgson et al., 2014; Zanker et al., 2024). The terminus position of Nordenskjöld Glacier has been relatively stable over the past century (Gordon et al., 2008; Cook et al., 2010). In more recent years, satellite imagery shows a retreat of $\sim$1 km between 2000 and 2019 (Tichit et al., 2024), suggesting a change in the balance between ablation and accumulation (Pfeffer, 2007; Bianchi et al., 2020). KHB hosts one major marine-terminating glacier, Briggs Glacier, which discharges directly into the fjord, as well as several smaller tributary glaciers along its southern shoreline. KHB is 13 km long, 3 km wide and $\leq$ 160 m deep. Several studies suggest accelerated retreat of glaciers over the past fifty years in South Georgia with glaciers on the northeast coast showing a greater rate of retreat compared to the southwest (Gordon et al., 2008; Hodgson et al., 2014; Farías-Barahona et al., 2020). The change from marine-terminating to land-terminating glaciers within the fjords of South Georgia could be significant for the amount and composition of trace elements, as has been shown in recent studies of Svalbard fjord (Herbert et al., 2020; Wehrmann et al., 2014). A recent study on the bioavailability of iron from terrestrial sources, such as meltwater from proglacial streams and groundwater from subaerial seepage at KHB and CBE, found that the latter is less bioavailable to phytoplankton (Stimpfle et al., 2026). Consequently, a substantial portion of the surface runoff entering both fjords appears to be in a bioavailable form capable of fuelling primary production (Stimpfle et al., 2026). This highlights the importance of freshwater export pathways from the fjords to the shelf and the open ocean. However, a comprehensive understanding of the water masses, the input of glacially derived nutrients, and the respective processes and feedbacks linking the nutrient cycle to recent climate change is lacking.

1.4 Nutrient utilisation and iron limitation in primary production

New production represents the proportion of total primary production supported by inputs of new nitrogen into the euphotic zone, which is predominantly supplied from deep waters (Whitney and Freeland, 1999). In a steady-state system where phytoplankton biomass is not rapidly changing, the amount of new production within the euphotic zone is thought to be in equilibrium with carbon export. Thus, estimates of carbon export potential may be derived through measurements of new production (Eppley and Peterson, 1979). The balance between primary production supported by nitrate (NO_3) versus ammonia (NH_4) and other forms of recycled nitrogen (referred to as regenerated production) can be described by the ratio of new production to total production (i.e., new production + regenerated production). The differentiation between new and regenerated production has led to the study of the mechanisms behind, and influence of, different nitrogen-based metabolic strategies in oceanic regimes and what they mean for carbon export potential.

Iron limitation prevents efficient utilization of macronutrients such as nitrate, phosphate and silica along with dissolved inorganic carbon. This inefficiency leads to the predominance of smaller-sized phytoplankton that mostly rely on recycled forms of nitrogen. The iron requirement for NH_4 uptake is substantially lower (1.6x Raven, 1988) than that of NO_3 uptake, causing a preference for NH_4 utilization by phytoplankton in Fe-limited regions (Geider and La Roche, 1994; Varela and Harrison, 1999). Additionally, high rates of regenerated production have been observed in small-celled phytoplankton with

https://doi.org/10.5194/egusphere-2026-1808
Preprint. Discussion started: 10 April 2026

low intracellular chlorophyll contents and larger surface area-to-volume ratios which enhance nutrient acquisition (Greene et al., 1992; Marchetti et al., 2006).

This paper aims to advance our understanding of South Georgia's hydrography and transport dynamics, with a specific focus on CBE and KHB. By introducing hydrographic and nutrient data from the fjords and the shelf in combination with current measurements we derive fjord circulation patterns and assess the nutrient exchange processes with the adjacent shelf region. Investigating these dynamics provides valuable insights into the fjord circulation during spring. In addition to presenting the physical oceanographic analysis of the fjord systems, this study provides context for the biological and geological datasets gathered during the same expedition. The paper is structured as follows: the data and methods for the hydrography, nutrients and current measurements are presented in Section 2, the results and discussion follow in Section 3, and we conclude with Section 4.

2 Data and methods

2.1 Hydrographic profiles

The data are gathered during the *PS133.2 Island Impact* cruise on board RV *Polarstern* in late austral spring between 20th November and 19th December 2022 at the stations shown in Fig. 2. The Conductivity-Temperature-Depth (CTD) casts are performed using a Seabird 911 CTD unit attached to a rosette of 24 Niskin water bottles of 12 l. The standard sensor configuration of the CTD system consists of two temperature, two conductivity, one pressure, two oxygen, and two fluorescence sensors (chl a and CDOM) as well as a transmissometer, and a photosynthetic active radiation (PAR) sensor. Most casts are performed from the surface to 10 m above the sea bed. Water samples are taken on the upcast. The data are processed according to AWI standard processing routines and averaged into 1 dbar pressure bins for analysis (Tippenhauer et al., 2023).

2.2 Nutrients

At each CTD station, unfiltered water samples are collected between 8 to 15 depths distributed throughout the water column. Samples are collected directly from Niskin bottles, into pre-cleaned (1M Hydrochloric acid) 50 ml sample bottles (High-density polyethylene) with screw caps. The sample bottles are previously rinsed three times with the sample. If possible, samples are measured on board immediately after sampling, else they are stored in a dark refrigerator for a maximum of 18 hours until measurement. Nitrate (NO_3) and nitrite (NO_2), phosphate (PO_4), silica (Si), and ammonia (NH_4) are measured using a flow-through autoanalyzer (AA500; Seal Analytical GmbH; Germany). The analytical methods are based on slightly modified methods of Grasshoff et al. (1999), except for ammonia, which is based on a fluorometric method developed by Kérouel and Aminot (1997). Calibration is performed in each run using MERCK standard solutions together with two different certified reference standards (CRM 7602a, CRM 7603a; JAMSTEC, Japan) to verify the accuracy and reproducibility of the system. Final calibration and validation is performed in the laboratory in Bremerhaven, Germany. The limits of quantitation

https://doi.org/10.5194/egusphere-2026-1808
Preprint. Discussion started: 10 April 2026

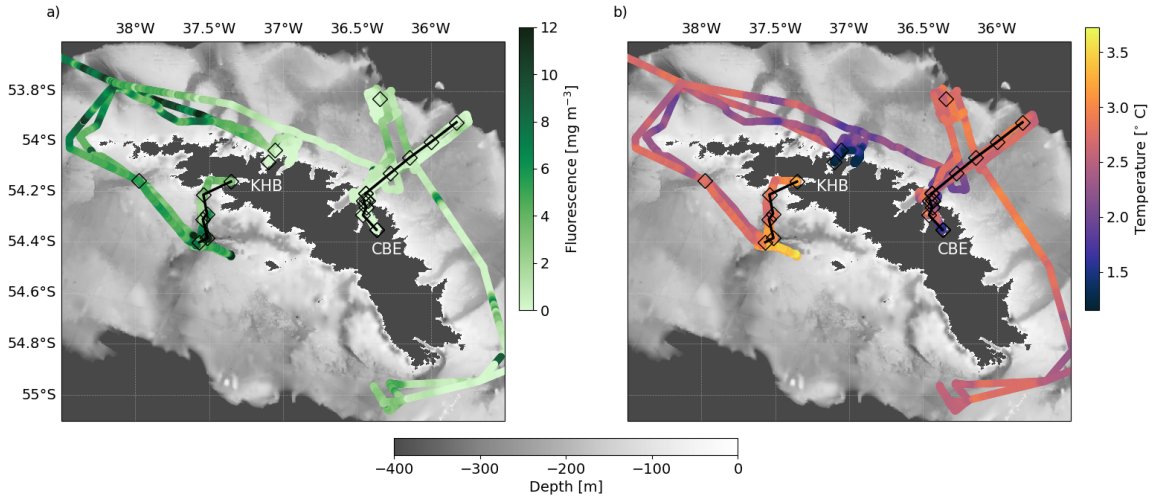

Figure 2. Underway surface a) fluorescence and b) temperature measurements of RV *Polarstern* providing an overview of the conditions in the study area. Bathymetry data (GEBCO Bathymetric Compilation Group 2023, 2023) of the South Georgia shelf (grey shading) and the locations of the CTD stations in Cumberland Bay East (CBE) and King Haakon Bay (KHB) shown. Black lines connect the stations in the respective fjords as used in the analysis in later sections.

(MDL) based on method blank values (EPA, 40 CFR Part 136) are (all in μmol l^{-1}) nitrate: 0.01, nitrite: 0.005, phosphate: 0.006, silica: 0.015, and ammonia: 0.02.

2.3 Measurements from shipboard instruments

The vessel-mounted Acoustic Doppler Current Profiler (VMADCP), the thermosalinograph and the ferrybox are located about 10 m below the surface. These instruments are monitored and calibrated by the shipboard's technician.

The VMADCP continuously collects profiles of ocean current velocity while underway. The RDI Ocean Surveyor instrument (150 KHBz) is mounted at an angle of 45 degrees and configured in narrowband mode with 4 m bin size, covering a range from 15 m to around 200 – 300 m depth depending on sea state, ship speed and the presence of back-scatterers in the water column. The data are processed using the 'ossi' software package developed by GEOMAR that implements the calibration of the misalignment angle between the VMADCP's transducers and the ship's forward direction.

https://doi.org/10.5194/egusphere-2026-1808
Preprint. Discussion started: 10 April 2026

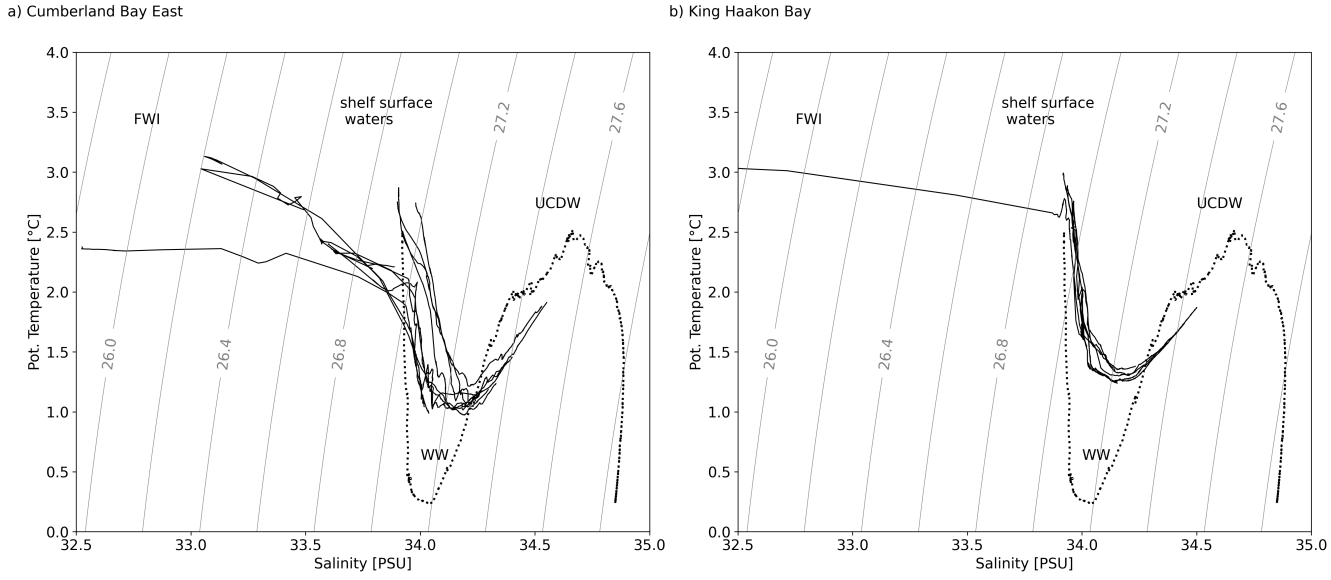

Figure 3. Temperature-Salinity diagram for a) Cumberland Bay East and b) King Haakon Bay stations and an off-shore profile for reference (dotted line). Isopycnals of the potential density anomaly (kg m^{-3}) are shown as gray contour lines. The four different water masses involved are Upper Circumpolar Deep Water (UCDW), Winter Water (WW), shelf-surface waters, and fresh water input (FWI).

Underway temperature is measured using two SBE21 thermosalinographs and two auxiliary SBE38 temperature sensors (Sea-Bird Scientific, USA) installed in the RV Polarstern flow-through system. Data are obtained from the DSHIP database at 1 s resolution, averaged to 1 min values, quality controlled, and corrected for sensor drift using post-season calibrations (Hoppmann et al., 2024). The underway fluorescence and sea surface temperature are shown in Fig. 2.

Weather data are collected throughout the cruise.The wind speeds mentioned in later sections correspond to the values recorded by the ship's weather station at 34 m above sea level.

3 Results and Discussion

The surface measurements allow for a first overview of the study region during the time of the cruise (Fig. 2); we discuss the fjords individually below. The highest fluorescence values of over 15 mg m^{-3} are reached in the western part of the study area and due south of KHB where the warmest surface temperatures of 3.7° C are also found (Fig. 2). By contrast, the lowest fluorescence values and slightly cooler surface waters are encountered on the eastern side of the island outside CBE ($\leq 1°$ C and ≤ 4 mg m^{-3}, respectively).

https://doi.org/10.5194/egusphere-2026-1808
Preprint. Discussion started: 10 April 2026

3.1 Water masses

The physical properties of the fjord and shelf-surface waters in CBE and KHB can be attributed to Upper Circumpolar Deep Water (UCDW), Winter Water (WW), and fresh water input (FWI) (Fig. 3). We define our four water masses according to the properties of the deep off-shelf profile (Fig. 3, dotted line). The deepest water mass is UCDW with 2.0°C < T < 2.6°C and 34.3 < S < 34.5 which is usually found at depths > 200 m in the Southern Ocean. The WW denotes the coldest water at a depth of roughly 120 m and likely consists of the remnant mixed layer of the previous year. Above the WW lies a warmer surface layer from seasonal heating (Brandon et al., 2000). We define the shelf surface waters with the value reached just below the surface with temperatures ranging from 2.5–3.5 °C as previously described by Brandon et al. (1999); Meredith et al. (2005) with temperatures of less than 3.5° C. The profiles closer to the glaciers inside the respective fjords display a fresher, cooler surface lens, attributable to various freshwater inputs (FWI), though the cold, fresh signature of subglacial discharge may not be retained due to plume entrainment (Carroll et al., 2015).

For stations in CBE the surface waters closest to the glaciers are influenced by cooler, fresher FWI (Fig. 3), reducing salinity to $\leq$ 32. The temperature minimum is at a depth of 100 to 150 m whilst salinity increases continuously with depth. Zanker et al. (2024, their Fig. 6) describe a clear signature of submarine ice melting in the surface waters from a previous summertime CTD survey (February 2020) in CBE, but we did not observe this in spring, when we might expect lower submarine melt rates compared to summer. Additionally, in our data, the closest measured station to the glacier is $\geq$ 2 km away from the calving front so that surface mixing may already have occurred and obscured the signal. In KHB only the station closest to the glacier has a FWI signal and the temperature of the WW in KHB is warmer compared to CBE.

3.2 Physical oceanography and nutrients

3.2.1 Cumberland Bay

The hydrography inside CBE appears to be highly influenced by bathymetry (Fig. 4). Moving from the calving front towards the fjord entrance (at 10 km) the isopycnals are sloping up at the surface and are mostly horizontal below 50 m showing the baroclinic structure. A freshwater signature (low salinity) is clearly visible near the glacier in the near-surface waters (Fig. 4b). On the shelf below 50 m the isopycnals slope up from the mouth towards the shelf break with a warm, salty water mass at depth. A fluorescence maximum of 2 mg m^{-3} matching low transmissivity is found on the shelf in 10 km distance from the fjord mouth. Since there are plenty of macronutrients we suspect other phytoplankton growth limitations such as iron, light or grazing. We also observe the warmest temperatures ($\geq$ 3°C, Fig. 4a) and a minimum ($\leq$ -10 μmol kg^{-1}) in the apparent oxygen utilization (AOU, which is used to infer respiration) at this location. Temperature ranges from 3°C at the surface on the shelf to 1°C near the sea bed inside the fjord. The temperature minimum marks the WW near the glacier and is located at 100–120 m depth which matches previous observations (e.g. Meredith, 2003; Brandon et al., 1999; Whitehouse et al., 1996). The maximum salinity is reached close to the sea bed on the shelf with 35 and the minimum of 31 at the surface closest to the glacier. The sill at 10 km from the glacier front at the fjord mouth has a high impact on the density structure. The depth is reduced to 180–200 m and the density increases due to decreasing temperature and increasing salinity. There is a fresher lens

https://doi.org/10.5194/egusphere-2026-1808
Preprint. Discussion started: 10 April 2026

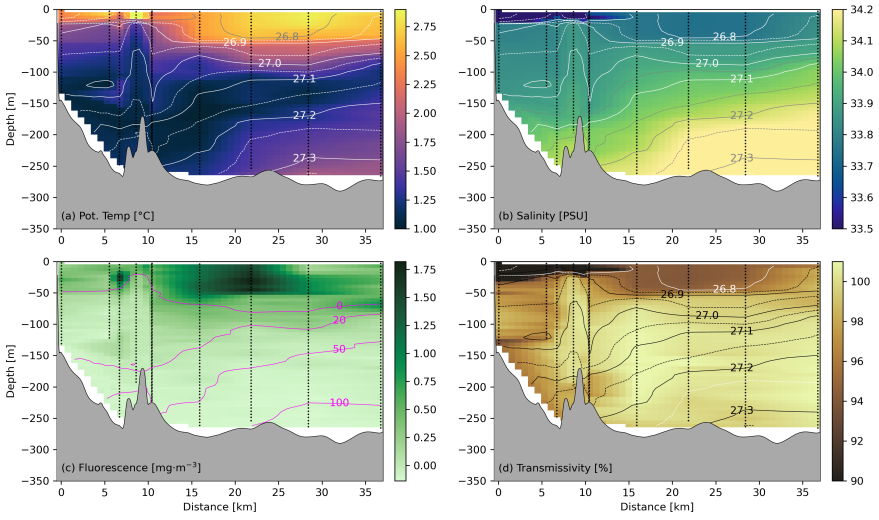

Figure 4. Hydrographic section of Cumberland Bay East from the glacier station (2 km from glacier) to the edge of the shelf. Sections for a) potential temperature, b) salinity, and c) fluorescence with apparent oxygen utilization isolines [μmol kg^{-1}], and d) transmissivity with isopycnals [kg m^{-3}]. Bathymetry is in grey (Hogg et al., 2016), shelf edge at 40 km.

near the surface and low primary production according to fluorescence and AOU. There is, however, a chlorophyll patch at 20 m depth right in front of the sill, suggesting that the sill acts like a barrier for fjord-shelf exchange at this depth. Further out on the shelf, the upsloping of the isopycnals towards the shelf edge are indicative of the transition from on-shelf to off-shelf waters as described by Brandon et al. (1999). The transmissivity (Fig. 4d) follows the isopycnals with a minimum in transmissivity in the fresh surface layer inside the fjord and increasing with depth. However, inside the fjord the values remain lower than on the shelf and the maximum values are reached at depth on the shelf.

NO_3 ranges from 24 μmol l^{-1} at the surface to 34 μmol l^{-1} at depth on the shelf (Fig. 5a). NO_2 has the highest values at the surface close to the glacier with 0.45 μmol l^{-1} decreasing to values of 0.05 μmol l^{-1} on the shelf at depth (Fig. 5b). The PO_4 distribution matches that of NO_3, with the highest values of 2.4 μmol l^{-1} at depth on the shelf and lower values of 1.7 μmol l^{-1} at the surface (Fig. 5c). Like NO_2, PO_4 is highest in the surface waters at the station close to the glacier, indicating that runoff may be a source. Surface runoff has been reported to deliver nutrient salts mobilized from bird guano deposits on land (Nędzarek, 2008). The higher PO_4 concentrations measured near the glacier could thus be influenced by guano-derived nutrient inputs, consistent with the exceptional seabird populations characteristic of South Georgia.

Si reaches the highest value of over 60 μmol l^{-1} at depth on the shelf and values of 20 μmol l^{-1} at the surface (Fig. 5d). Values of NH_4 range between 0.1 μmol l^{-1} at depth on the shelf and roughly 1 μmol l^{-1} close to the glacier and at a depth of 80-100 m, which coincides with the thermocline (Fig. 5e). The maximum values of NH_4 correspond to the 0 and 10 μmol l^{-1} AOU contours (Fig. 5f). In general the relatively high concentrations suggest that the phytoplankton have plenty of macronutrients. With the exception of NO_2 the macronutrients are also strongly correlated to salinity, AOU and fluorescence.

https://doi.org/10.5194/egusphere-2026-1808
Preprint. Discussion started: 10 April 2026

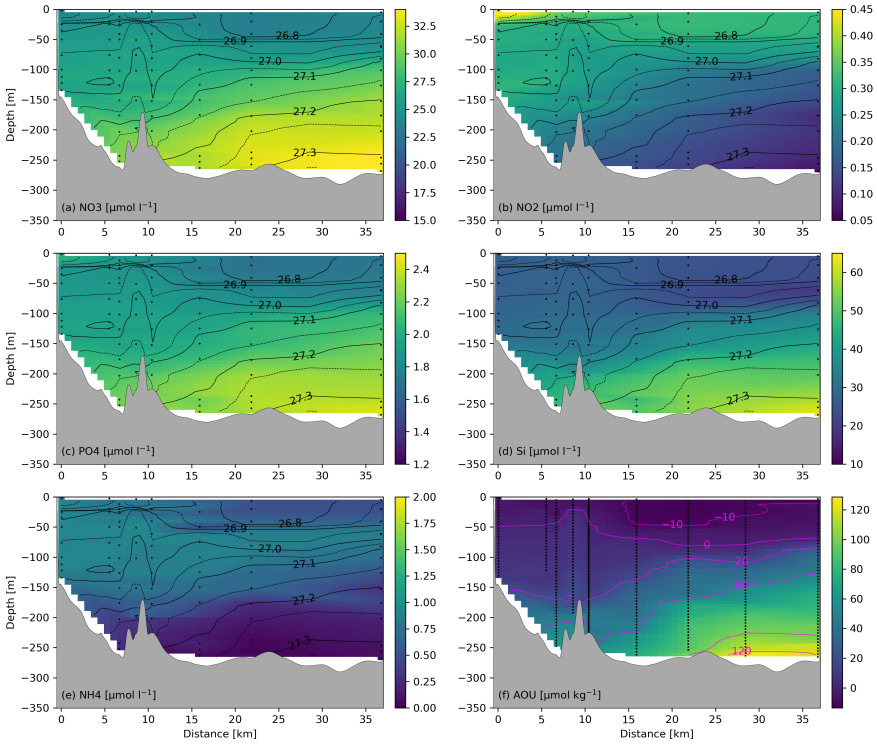

Figure 5. Nutrients along Cumberland Bay East section from the glacier station (2 km from glacier) to the edge of the shelf. Sections for a) nitrate, b) nitrite, c) phosphate, d) silica, e) ammonia, and f) apparent oxygen utilization with isolines (pink). Black dots indicate the location of the stations and depth of the water sampling. Black contours are isopycnals [kg m^{-3}], and bathymetry is in grey (Hogg et al., 2016).

Since there is plenty of NO_3, PO_4 and Si in the surface waters, the relatively low phytoplankton biomass is likely explained by other growth limiting factors such as light or micronutrients such as iron or top-down removal by grazers.

3.2.2 King Haakon Bay

The hydrographic profiles in KHB reveal different properties of the water column compared to CBE (Fig. 6). As with CBE, the transect goes from inside the fjord out onto the shelf. For this transect, the isopycnals are horizontal for the whole transect with the exception of a small signature of increased surface density in the upper 20 m just outside the fjord 10 km along the section. The bathymetry in KHB is very different compared to CBE and does seemingly not influence the water structure as it does in CBE. Temperatures are warmer and the minimum is reached outside the fjord at around 150 m depth, indicative of the WW layer. Again, as CBE, we observed slightly warmer waters towards the sea bed on the shelf (Fig. 6a) which coincides with the highest values in salinity indicative of UCDW instrusion (Fig. 6b). Besides the clear layering of density, the most striking difference to CBE are the much higher fluorescence and lower AOU values indicating much higher phytoplankton productivity (Fig. 6c). Fluorescence reaches 14 mg m^{-3} and AOU decreases to -60 μmol kg^{-1}, one reason could be the local alleviation

https://doi.org/10.5194/egusphere-2026-1808
Preprint. Discussion started: 10 April 2026

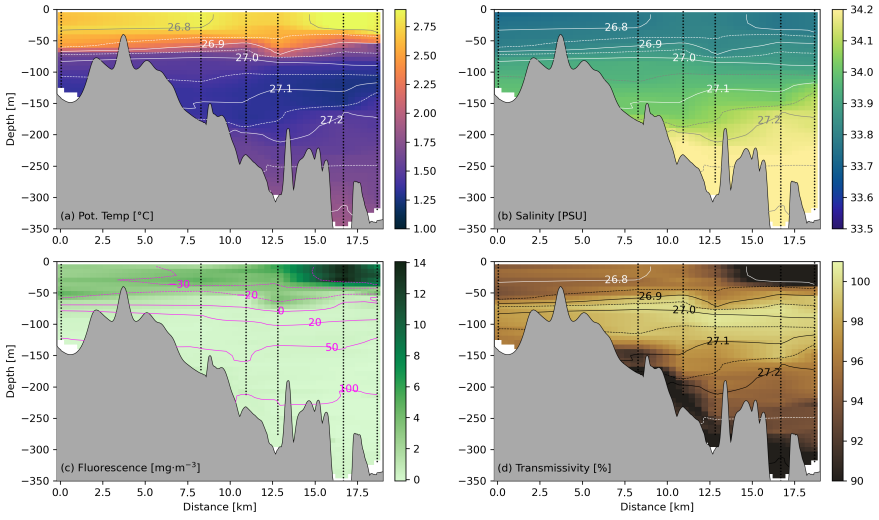

Figure 6. Hydrographic section of King Haakon Bay from the glacier station to the edge of the shelf. Sections for a) potential temperature, b) salinity, and c) fluorescence with apparent oxygen utilization isolines [μmol kg^{-1}], and d) transmissivity with isopycnals [kg m^{-3}]. Bathymetry is in grey (Hogg et al., 2016)

of iron limitation. The highest fluorescence values are observed out on the shelf, furthest away from the entrance to KHB.The transmissivity reaches the highest values at the thermocline, the depth of the WW (Fig. 6d). In contrast to CBE, towards the surface and towards the sea bed the transmissivity decreases with the smallest values in the surface layer out on the shelf, which coincide with the chlorophyll bloom. There is also reduced transmissivity close to sea bed, a possible indicator for a soft transition from water to sediment.

The results for the nutrient measurements in KHB show that NO_3 increases from 15 μmol l^{-1} at the surface to 33 μmol l^{-1} at depth on the shelf (Fig. 7a), and is negatively correlated with the fluorescence, likely due to draw down by the phytoplankton. NO_2 displays the highest values of 0.45 μmol l^{-1} at the surface close to the glacier and, similar to CBE decreases with depth (Fig. 7b). PO_4 is distributed similarly to NO_3, with highest values of 2.4 μmol l^{-1} at depth on the shelf and lower values of 1.2 μmol l^{-1} at the surface (Fig. 7c). In contrast to CBE, however, there is no indication for PO_4 input close to the glacier. Si also reaches high values of over 60 μmol l^{-1} at depth on the shelf, similar to CBE, but even lower values of 10 μmol l^{-1} at the surface (Fig. 7d). Values of NH_4 range between 0 μmol l^{-1} at depth on the shelf and 2 μmol l^{-1} (twice as much as in CBE) close to the glacier and at a depth of 50-80 m, close to the thermocline (Fig. 7e). The maximum values of NH_4 correspond to the 0 μmol kg^{-1} AOU contour and suggest high rates of bacterial remineralization.

The particulate N to Si ratio of diatoms is $\sim$ 1 (Brzezinski, 2004) and thus, high ratios of dissolved NO_3 to silicate could indicate potential silicate limitation. Dissolved N:Si ratios have a mean value of 0.86, very similar to CBE. However, above 50 m these ratios are overwhelmingly above 1, reaching 1.6. Furthermore, these values correspond to elevated fluorescence values

https://doi.org/10.5194/egusphere-2026-1808
Preprint. Discussion started: 10 April 2026

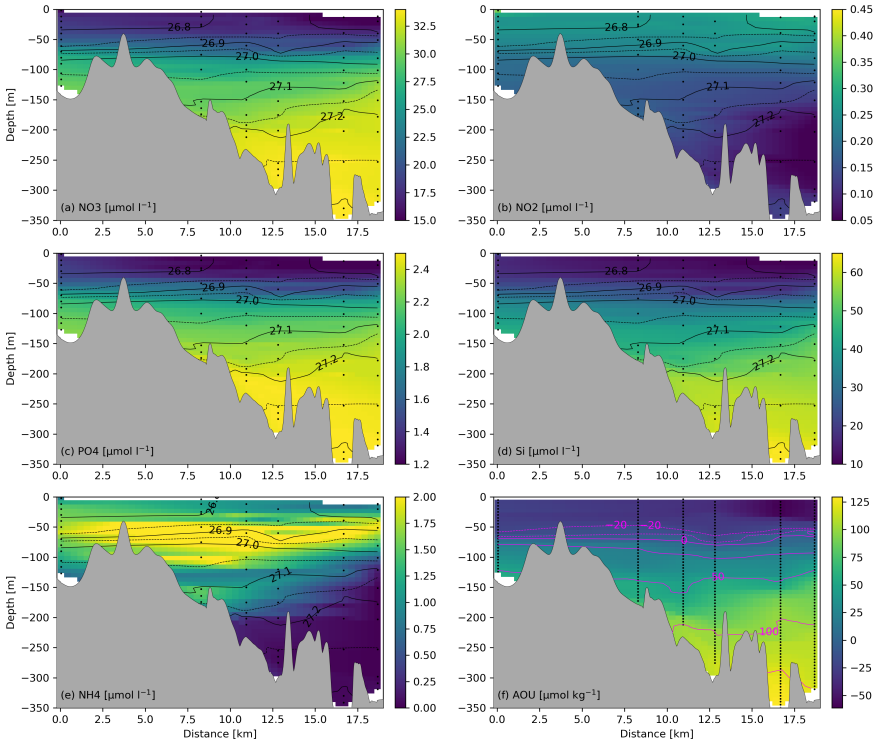

Figure 7. Nutrients along King Haakon Bay section from the glacier station to the edge of the shelf. Sections for a) nitrate, b) nitrite, c) phosphate, d) silica, e) ammonia, and f) apparent oxygen utilization with isolines (pink). Black dots indicate the location of the stations and depth of the water sampling. Black contours are isopycnals [kg m^{-3}], and bathymetry is in grey (Hogg et al., 2016).

and, thus, suggest that the phytoplankton community, consisting mostly of diatoms (Stimpfle et al., 2026) is likely running into silicate limitation.

NO_3, PO_4 and Si are strongly ($\rho \geq 0.95$) positively correlated while NO_2, again does not follow this trend and is negatively ($\rho \leq$ -0.95) correlated to those three.

NO_3, NO_2, PO_4 and Si are also strongly negatively correlated to the salinity, AOU and fluorescence. NO_3 is plentiful and not limiting. Since NH_4 can be consumed and produced during these blooms it shows no correlation to any other biological or physical parameter.

3.3 Transport and Circulation

3.3.1 Geostrophic circulation and wind forcing

We explore whether the CBE and KHB fjords are wide enough to develop a stable geostrophic circulation by relating the Rossby radius to the basin's diameter (Cottier et al., 2010).

https://doi.org/10.5194/egusphere-2026-1808
Preprint. Discussion started: 10 April 2026

The smallest value we compute is $\sim$ 2 km inside the fjords and the largest is $\sim$ 4 km closer to the glacier resulting in a mean Rossby radius of $\sim$ 3 km. In context with the topography of the fjords studied here (Hodgson et al., 2014; Hogg et al., 2016), we conclude that it is unlikely that a geostrophically stable current (featuring an inflow on one side and an outflow on the other) develops in the 3–5 km wide fjords, which is also in agreement with Zanker et al. (2024).

During the period of the voyage, the wind comes primarily from the west/northwest direction. In CBE the median (to reduce the impact of outliers) of the wind speed data gathered while in the area is 10.7 m s^{-1} from north-northwest. These values are in agreement with the climatology of surface winds at the weather station at KEP (54.283° S, 36.495° W) in CBE which record westerly winds of 7.5–15 m s^{-1} in austral spring (Hosking et al., 2015). On the western side of the island in KHB the winds have a median speed of 9.4 m s^{-1} from the west. The higher wind speeds and variations in wind direction on the eastern side of the island might be explained by lee effects or the time difference of sampling. The cross-fjord structure of outflow is driven by the winds and the orientation of the fjord arms with respect to the dominant northwestward shelf flows. As other fjord studies have found, the winds have the possibility to drive significant oceanographic variability on time scales of days (Jackson et al., 2014).

3.3.2 Tides

Another important driver of circulation are tides. Using the OSU Tidal Prediction Software OTPS (Egbert and Erofeeva, 2002), we compute the tides on the shelf and in front of the CBE and KHB fjord systems for the sampling period. The maximum tidal elevation of the principal tidal component M_2 is in the range 30–50 cm for the two different fjords. From this we compute the flow velocity inside the fjords caused by tides. Assuming a homogeneous tidal elevation throughout the fjord, we compute the flow necessary to support an elevation gain of $2 \cdot M_2$ per transition from high to low tide. Illustrating this for CBE and taking into account the size of the fjord (width 3–5 km, length approx. 15 km, and an average depth of 200 m (Hodgson et al., 2014)) the tidal flow is approximately 1620 m^3 s^{-1} at the mouth of the fjord. This corresponds to an average horizontal velocity of 0.2 cm s^{-1} across the mouth of the fjord and a horizontal water parcel displacement of 40 m during the transition from high to low tide. Similar magnitude is estimated for KHB. Supporting this estimate is the work by Meredith (2003) who extracted a tidal meridional component of less than 2 cm s^{-1} and a zonal component of less than 0.5 cm s^{-1} on the surrounding shelf and open ocean from their VMADCP measurements. Modeling studies (e.g. Young et al., 2014; Zanker et al., 2024) suggest that tides have little influence on fjord circulation and this is supported by our estimate.

3.3.3 VMADCP measurements

The currents inside the fjord are generally too weak ($\leq$ 0.2 m s^{-1}) to separate actual currents from ship movement in the VMADCP data. To improve signal to noise ratio we focus on measurements when on station and thus minimal ship movements during the time series. We use the data to validate our previous estimates on tides and to constrain the residence time of particles and water parcels inside the fjord before they exit onto the shelf.

The longest time series (13 hours) is obtained at the glacier station in CBE. According to the tidal model (Egbert and Erofeeva, 2002), this period includes the transition from low to high tide. As expected, the data does not show a tidal signature.

https://doi.org/10.5194/egusphere-2026-1808
Preprint. Discussion started: 10 April 2026

The average over the entire time series indicates an inflow (0.03 m s^{-1}) in the upper water layer (-27 m to -55 m) and weak outflow in the bottom layer (-87 m to -115 m). The difference in magnitude and direction between the top and bottom layer supports the presence of a vertical overturning circulation. Comparison with the wind pattern for that day, which is consistently from the northwest, suggests that the upper surface flow towards the glacier may be wind-driven, leading to decoupling from the bottom layer. We estimate the total in- and outflow (Fig.8a) using a transect along the sill at the fjord mouth (Fig. 8b). Looking at the sill section at 10 km, there is an outflow of up to 0.14 m s^{-1} in the top 50 m and an inflow below 100 m of up to 0.1 m s^{-1}. The available data are in a distance of 500 m to the coast. This matches the freshwater signal detected in the CTD casts (Fig. 4) and even though we cannot trace back the complete flow pattern from sill to glacier, the measurements above the sill suggest that there is transport of freshwater, particles and nutrients out of the fjord over the sill. This is also apparent in the sloping of the isopycnals (Fig. 8a, black lines), which show the decreasing density in the surface layer with fresher water transported over the sill towards the shelf and shelf water entering the fjord close to the sea bed. Since a VMADCP can only measure the top 90 % of the water column we lack measurements near the sea bed. The data indicate an outflow in the top 50 m over a distance of 1 km at 0.1 m s^{-1}, corresponding to 5000 m^3 s^{-1}. From this we estimate the residence time of particles, nutrients and water parcels. For the entire basin to be exchanged, assuming constant flow and neglecting mixing with inflowing water, the process would take approximately 2 years (fjord geometry: 15 km length, 3 km width, 200 m depth). However, taking into account the transmissivity data (Fig. 4d) we limit the transported water mass to the top 30 m, where transmissivity is lowest and most particles are located. For this volume of water to be transported over 15 km to the shelf would take 3 days. Zanker et al. (2024) found spring time depth-averaged velocities of ∼0.02 m s^{-1} within the fjord. A particle at the calving front, travelling 15 km to reach the shelf, would take 6 days at that speed. They also performed particle tracking for fish larvae constrained to the upper 100 m, which suggest similar transit times (personal comm.). Therefore, iron released at the marine-terminating glacier into the surface layer, without disturbance from eddies or vertical mixing, could reach the shelf within 3 to 6 days. In contrast, iron introduced by benthic fluxes, subject to coastal inflow, vertical mixing, and horizontal stirring could take months to reach the shelf. This is an important factor to consider as in addition to direct input from the glacier, abiotic and biotic processes in sediments may also be an important source of iron to the overlying water column. It is likely that in the timescale of months, not much of the liberated iron will reach the shelf to trigger and sustain phytoplankton blooms. The residence time of iron is, therefore, dependent on the source and depth from where it is released into the water column. However, benthic iron flux calculations indicate generally higher iron efflux and more dynamic depositional conditions at KHB compared to CB, primarily driven by enhanced organic carbon accumulation rates (Ebner et al., under review at Global Biogeochemical Cycles). This suggests that, despite potentially slow lateral transport, abiotic and biotic processes in the uppermost part of the sediment may represent a substantial local source of dissolved iron to the overlying water column. In addition, Zanker et al. (2024) found seasonal variability in fjord circulation with stronger currents in austral summer, therefore, the residence time may be sensitive to the seasonal timing of release and further understanding would be gained by taking measurements from different seasons.

For KHB, only two stations are located inside the fjord, which is insufficient to fully constrain the flow. However, the total flow velocity at the station closest to the glacier is approximately 0.04 m s^{-1}. Therefore, the residence time for particles in the upper water layer is likely on the order of days, similar to CBE.

https://doi.org/10.5194/egusphere-2026-1808
Preprint. Discussion started: 10 April 2026

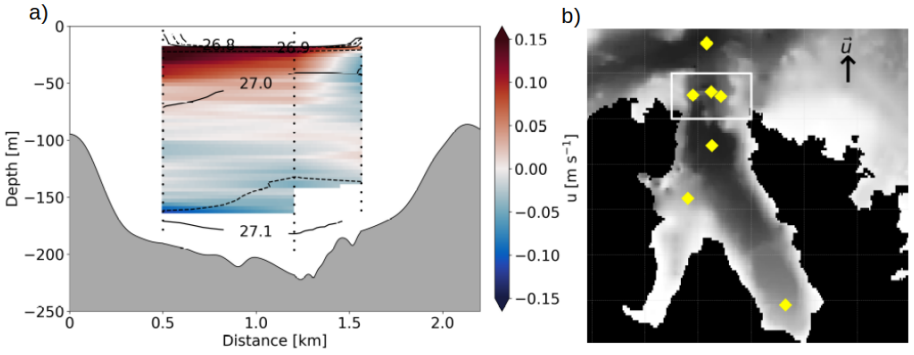

Figure 8. a) Along fjord velocities ($\boldsymbol{u}$) in Cumberland Bay East over the sill linearly interpolated between the stations where the ship speed is close to zero along the transect, red is outflow, blue inflow. Bathymetry is gray (Hogg et al., 2016) and isopycnals black (dotted lines being the values halfway between those of the solid lines). The transect is from the bordering western coast towards the east. b) The geographical locations of the stations along Cumberland Bay East sill (white box), with the along-fjord direction (u) indicated.

4 Conclusions

The Southern Ocean is a high-nutrient, low-chlorophyll region, however, recurring chlorophyll blooms have been observed downstream of the island of South Georgia. South Georgia is believed to play a major role in introducing iron to the system, which drives the development of these intense blooms. Glaciers, rivers, sediments and dust are all possible sources of iron. While it is important to find and quantify these sources the physical processes transporting water masses and therefore iron and nutrients from the sources to the observed bloom also play a leading order control on the blooms. In this study, we investigated transport from inside the fjords onto the continental shelf and the timescales.

With the data collected during *Island Impact* in late austral spring 2022 on RV *Polarstern* we identify the different water masses inside the fjords and on the surrounding shelf. Bathymetry is important in steering the circulation as we see in CBE. Not so much in KHB, so its hard to generalise the results. The measurements on the shelf are consistent with previous studies, validating the suitability of numerical models in representing circulation and hydrography accurately. Models predict weak tides in the vicinity of the fjords which is confirmed by this study and the Rossby radius inside the fjords is too large to allow a stable horizontal geostrophic circulation with an inflow and an outflow on separate sides of the fjord.

In CBE the export of fjord waters onto the shelf is weak (max values of 0.15 m s^{-1} over the sill) without strong tidal or geostrophic forcing resulting in a weak vertical overturning circulation. Complementing our measurements with previous model results we conclude a minimum residence time in CBE for particles released close to the glacier at the surface of 6 days, neglecting the effects of vertical mixing or horizontal stirring. For particles released closer to the sea bed and those from benthic fluxes we infer a residence time of the order of months. King Haakon Bay (KHB) by comparison is smaller and the highest temperatures and chlorophyll values are recorded on the shelf. With these two different fjord systems we demonstrate the diversity of the local environment. This paper is part of a series and future work examining the biological and geochemical measurements from *Island Impact* will deepen our understanding of the South Georgia island system and its role in fertilizing

https://doi.org/10.5194/egusphere-2026-1808
Preprint. Discussion started: 10 April 2026

the ocean. The data were collected in November to December 2022 and are therefore limited to this season and year. However, we have shown that the major physical process of water mass exchange happens via a vertical overturning circulation, steered by bathymetry and influenced by the winds. The Rossby radius, and tides might change throughout the year, so that our findings are more representative for the fjord/shelf exchange in spring. To improve these first estimates of residence time inside the fjord and possible seasonal and interannual variability a long-term, widely distributed oceanographic dataset would be required. However, in this study we demonstrate the physical processes leading to transport onto the continental shelf with implications for the supply of iron to downstream chlorophyll blooms.

Data availability. The thermosalinograph data used in this study are available on Pangaea at (Hoppmann et al., 2024). Bathymetry data were obtained from GEBCO Compilation Group (2023) GEBCO 2023 Grid (https://doi.org/10.5285/b8143952-421c-4544-8437-58f339253d30). Processed CTD and nutrient profiles and the VMADCP data can be accessed through Oetjens (2025) and Tippenhauer et al. (2023).

https://doi.org/10.5194/egusphere-2026-1808
Preprint. Discussion started: 10 April 2026

Author contributions. This scientific paper is a product of collaborative efforts by the authors. AO led the conceptualization, data curation, formal analysis, visualization, and initial draft writing. WJvA conducted formal analyses of the oceanographic data, supervised, and edited the draft. JA contributed to investigations, conceptualization, and editing. BE focused on editing and conceptualization of the geochemical aspects. FK conducted formal analysis of the nutrient data and contributed to the initial draft. KUL conducted investigations and data curation of the nutrient measurements. RM contributed to the visualization of Figure 1. SK handled project administration and funding acquisition. All authors reviewed the original draft to ensure its quality.

Competing interests. The authors declare that they have no conflict of interest.

Acknowledgements. We thank the captain, crew and scientific party of RV *Polarstern* cruise PS133.2 for their support of this work. Data for this study was collected under grant number AWI_PS133/2_10 and Grant No. AWI_PS133/2_13. J.A.'s participation in the cruise was partly funded by a Doctoral Training Partnership studentship from the UK Natural Environmental Research Council. The contribution of EY was funded by British Antarctic Survey National Capability funding to the Polar Oceans science programme. The contribution of JZ was supported by the Natural Environment Research Council via the British Antarctic Survey Polar Oceans program and the INSPIRES Doctoral Training Partnership.

https://doi.org/10.5194/egusphere-2026-1808
Preprint. Discussion started: 10 April 2026

References

Bakker, D. C., Nielsdóttir, M. C., Morris, P. J., Venables, H. J., and Watson, A. J.: The island mass effect and biological carbon uptake for the subantarctic Crozet Archipelago, Deep Sea Research Part II: Topical Studies in Oceanography, 54, 2174–2190, https://doi.org/10.1016/j.dsr2.2007.06.009, 2007.

Behrenfeld, M. J., Bale, A. J., Kolber, Z. S., Aiken, J., and Falkowski, P. G.: Confirmation of iron limitation of phytoplankton photosynthesis in the equatorial Pacific Ocean, Nature, 383, 508–511, https://doi.org/10.1038/383508a0, 1996.

Bianchi, T. S., Arndt, S., Austin, W. E., Benn, D. I., Bertrand, S., Cui, X., Faust, J. C., Koziorowska-Makuch, K., Moy, C. M., Savage, C., Smeaton, C., Smith, R. W., and Syvitski, J.: Fjords as Aquatic Critical Zones (ACZs), Earth-Science Reviews, 203, 103 145, https://doi.org/10.1016/j.earscirev.2020.103145, 2020.

Blain, S., Tréguer, P., Belviso, S., Bucciarelli, E., Denis, M., Desabre, S., Fiala, M., Martin Jézéquel, V., Le Fèvre, J., Mayzaud, P., Marty, J.-C., and Razouls, S.: A biogeochemical study of the island mass effect in the context of the iron hypothesis: Kerguelen Islands, Southern Ocean, Deep Sea Research Part I: Oceanographic Research Papers, 48, 163–187, https://doi.org/10.1016/S0967-0637(00)00047-9, 2001.

Borrione, I. and Schlitzer, R.: Distribution and recurrence of phytoplankton blooms around South Georgia, Southern Ocean, Biogeosciences, 10, 217–231, https://doi.org/10.5194/bg-10-217-2013, 2013.

Borrione, I., Aumont, O., Nielsdóttir, M. C., and Schlitzer, R.: Sedimentary and atmospheric sources of iron around South Georgia, Southern Ocean: a modelling perspective, Biogeosciences, 11, 1981–2001, https://doi.org/10.5194/bg-11-1981-2014, 2014.

Boyd, P. W., Claustre, H., Levy, M., Siegel, D. A., and Weber, T.: Multi-faceted particle pumps drive carbon sequestration in the ocean, Nature, 568, 327–335, https://doi.org/10.1038/s41586-019-1098-2, 2019.

Brandon, M. A., Murphy, E. J., Whitehouse, M. J., Trathan, P. N., Murray, A. W., Bone, D. G., and Priddle, J.: The shelf break front to the east of the sub-Antarctic island of South Georgia, Continental Shelf Research, 19, 799–819, https://doi.org/10.1016/S0278-4343(98)00112-5, 1999.

Brandon, M. A., Murphy, E. J., Trathan, P. N., and Bone, D. G.: Physical oceanographic conditions to the northwest of the sub-Antarctic Island of South Georgia, Journal of Geophysical Research: Oceans, 105, 23 983–23 996, https://doi.org/10.1029/2000JC900098, 2000.

Brzezinski, M. A.: The Si:C:N ratio of marine diatoms: Interspecific variability and the effect of some environmental variables, Journal of Phycology, 21, 347–357, https://doi.org/10.1111/j.0022-3646.1985.00347.x, 2004.

Carroll, D., Sutherland, D. A., Shroyer, E. L., Nash, J. D., Catania, G. A., and Stearns, L. A.: Modeling Turbulent Subglacial Meltwater Plumes: Implications for Fjord-Scale Buoyancy-Driven Circulation, Journal of Physical Oceanography, 45, 2169–2185, https://doi.org/10.1175/JPO-D-15-0033.1, 2015.

Coale, K. H., Johnson, K. S., Fitzwater, S. E., Gordon, R. M., Tanner, S., Chavez, F. P., Ferioli, L., Sakamoto, C., Rogers, P., Millero, F., Steinberg, P., Nightingale, P., Cooper, D., Cochlan, W. P., Landry, M. R., Constantinou, J., Rollwagen, G., Trasvina, A., and Kudela, R.: A massive phytoplankton bloom induced by an ecosystem-scale iron fertilization experiment in the equatorial Pacific Ocean, Nature, 383, 495–501, https://doi.org/10.1038/383495a0, 1996.

Cook, A., Poncet, S., Cooper, A., Herbert, D., and Christie, D.: Glacier retreat on South Georgia and implications for the spread of rats, Antarctic Science, 22, 255–263, https://doi.org/10.1017/S0954102010000064, 2010.

Copernicus Marine Service and PML: Global Ocean Colour Plankton MY L4 monthly observations, https://doi.org/10.48670/MOI-00283, 2022.

https://doi.org/10.5194/egusphere-2026-1808
Preprint. Discussion started: 10 April 2026

Cottier, F. R., Nilsen, F., Skogseth, R., Tverberg, V., Skarðhamar, J., and Svendsen, H.: Arctic fjords: a review of the oceanographic environment and dominant physical processes, Geological Society, London, Special Publications, 344, 35–50, https://doi.org/10.1144/SP344.4, 2010.

Egbert, G. D. and Erofeeva, S. Y.: Efficient Inverse Modeling of Barotropic Ocean Tides, Journal of Atmospheric and Oceanic Technology, 19, 183–204, https://doi.org/10.1175/1520-0426(2002)019<0183:EIMOBO>2.0.CO;2, 2002.

Eppley, R. W. and Peterson, B. J.: Particulate organic matter flux and planktonic new production in the deep ocean, Nature, 282, 677–680, https://doi.org/10.1038/282677a0, publisher: Nature Publishing Group, 1979.

Farías-Barahona, D., Sommer, C., Sauter, T., Bannister, D., Seehaus, T. C., Malz, P., Casassa, G., Mayewski, P. A., Turton, J. V., and Braun, M. H.: Detailed quantification of glacier elevation and mass changes in South Georgia, Environmental Research Letters, 15, 034 036, https://doi.org/10.1088/1748-9326/ab6b32, publisher: IOP Publishing, 2020.

GEBCO Bathymetric Compilation Group 2023: The GEBCO_2023 Grid - a continuous terrain model of the global oceans and land., https://doi.org/10.5285/F98B053B-0CBC-6C23-E053-6C86ABC0AF7B, 2023.

Geider, R. J. and La Roche, J.: The role of iron in phytoplankton photosynthesis, and the potential for iron-limitation of primary productivity in the sea, Photosynthesis Research, 39, 275–301, https://doi.org/10.1007/BF00014588, 1994.

Gordon, J. E., Haynes, V. M., and Hubbard, A.: Recent glacier changes and climate trends on South Georgia, Global and Planetary Change, 60, 72–84, https://doi.org/10.1016/j.gloplacha.2006.07.037, 2008.

Grasshoff, K., Kremling, K., and Ehrhardt, M., eds.: Methods of Seawater Analysis, Wiley, 1 edn., ISBN 978-3-527-29589-0 978-3-527-61398-4, https://doi.org/10.1002/9783527613984, 1999.

Greene, R. M., Geider, R. J., Kolber, Z., and Falkowski, P. G.: Iron-Induced Changes in Light Harvesting and Photochemical Energy Conversion Processes in Eukaryotic Marine Algae 1, Plant Physiology, 100, 565–575, https://doi.org/10.1104/pp.100.2.565, 1992.

Herbert, L. C., Riedinger, N., Michaud, A. B., Laufer, K., Røy, H., Jørgensen, B. B., Heilbrun, C., Aller, R. C., Cochran, J. K., and Wehrmann, L. M.: Glacial controls on redox-sensitive trace element cycling in Arctic fjord sediments (Spitsbergen, Svalbard), Geochimica et Cosmochimica Acta, 271, 33–60, https://doi.org/10.1016/j.gca.2019.12.005, 2020.

Hodgson, D. A., Graham, A. G., Griffiths, H. J., Roberts, S. J., Cofaigh, C. O., Bentley, M. J., and Evans, D. J.: Glacial history of sub-Antarctic South Georgia based on the submarine geomorphology of its fjords, Quaternary Science Reviews, 89, 129–147, https://doi.org/10.1016/j.quascirev.2013.12.005, 2014.

Hogg, O. T., Huvenne, V. A. I., Griffiths, H. J., Dorschel, B., and Linse, K.: Landscape mapping at sub-Antarctic South Georgia provides a protocol for underpinning large-scale marine protected areas, Scientific Reports, 6, 33 163, https://doi.org/10.1038/srep33163, 2016.

Hoppmann, M., Tippenhauer, S., and Kasten, S.: Continuous thermosalinograph oceanography along RV POLARSTERN cruise track PS133/2, https://doi.org/10.1594/PANGAEA.964289, backup Publisher: Alfred Wegener Institute, Helmholtz Centre for Polar and Marine Research, Bremerhaven Type: dataset, 2024.

Hosking, J. S., Bannister, D., Orr, A., King, J., Young, E., and Phillips, T.: Orographic disturbances of surface winds over the shelf waters adjacent to South Georgia: Orographic disturbances of surface winds around South Georgia, Atmospheric Science Letters, 16, 50–55, https://doi.org/10.1002/asl2.519, 2015.

Jackson, R. H., Straneo, F., and Sutherland, D. A.: Externally forced fluctuations in ocean temperature at Greenland glaciers in non-summer months, Nature Geoscience, 7, 503–508, https://doi.org/10.1038/ngeo2186, publisher: Nature Publishing Group, 2014.

Koenig, Z., Provost, C., Park, Y., Ferrari, R., and Sennéchael, N.: Anatomy of the Antarctic Circumpolar Current volume transports through Drake Passage, Journal of Geophysical Research: Oceans, 121, 2572–2595, https://doi.org/10.1002/2015JC011436, 2016.

https://doi.org/10.5194/egusphere-2026-1808
Preprint. Discussion started: 10 April 2026

Korb, R., Whitehouse, M., Atkinson, A., and Thorpe, S.: Magnitude and maintenance of the phytoplankton bloom at South Georgia: a naturally iron-replete environment, Marine Ecology Progress Series, 368, 75–91, https://doi.org/10.3354/meps07525, 2008.

Korb, R. E. and Whitehouse, M.: Contrasting primary production regimes around South Georgia, Southern Ocean: large blooms versus high nutrient, low chlorophyll waters, Deep Sea Research Part I: Oceanographic Research Papers, 51, 721–738, https://doi.org/10.1016/j.dsr.2004.02.006, 2004.

Korb, R. E., Whitehouse, M. J., Thorpe, S. E., and Gordon, M.: Primary production across the Scotia Sea in relation to the physico-chemical environment, Journal of Marine Systems, 57, 231–249, https://doi.org/10.1016/j.jmarsys.2005.04.009, 2005.

Kérouel, R. and Aminot, A.: Fluorometric determination of ammonia in sea and estuarine waters by direct segmented flow analysis, Marine Chemistry, 57, 265–275, https://doi.org/10.1016/S0304-4203(97)00040-6, 1997.

Marchetti, A., Sherry, N. D., Kiyosawa, H., Tsuda, A., and Harrison, P. J.: Phytoplankton processes during a mesoscale iron enrichment in the NE subarctic Pacific: Part I—Biomass and assemblage, Deep Sea Research Part II: Topical Studies in Oceanography, 53, 2095–2113, https://doi.org/10.1016/j.dsr2.2006.05.038, 2006.

Martin, J. H.: Glacial-interglacial CO change: The Iron Hypothesis, Paleoceanography, 5, 1–13, https://doi.org/10.1029/PA005i001p00001, 1990.

Martin, J. H., Gordon, R. M., and Fitzwater, S. E.: Iron in Antarctic waters, Nature, 345, 156–158, https://doi.org/10.1038/345156a0, 1990.

Matano, R. P., Combes, V., Young, E. F., and Meredith, M. P.: Modeling the Impact of Ocean Circulation on Chlorophyll Blooms Around South Georgia, Southern Ocean, Journal of Geophysical Research: Oceans, 125, https://doi.org/10.1029/2020JC016391, 2020.

Meredith, M. P.: Southern ACC Front to the northeast of South Georgia: Pathways, characteristics, and fluxes, Journal of Geophysical Research, 108, 3162, https://doi.org/10.1029/2001JC001227, 2003.

Meredith, M. P., Brandon, M. A., Murphy, E. J., Trathan, P. N., Thorpe, S. E., Bone, D. G., Chernyshkov, P. P., and Sushin, V. A.: Variability in hydrographic conditions to the east and northwest of South Georgia, 1996–2001, Journal of Marine Systems, 53, 143–167, https://doi.org/10.1016/j.jmarsys.2004.05.005, 2005.

Mole, R., von Appen, W. J., Becker, H., Haumann, F. A., Kanzow, T., Piñango, A., Stimpfle, J., Trimborn, S., and Young, E. F.: Wind-Driven Iron Supply by Ekman Buoyancy Flux Enhances Phytoplankton Bloom in the Antarctic Circumpolar Current, Journal of Geophysical Research: Oceans, 130, e2025JC022 530, https://doi.org/10.1029/2025JC022530, _eprint: https://agupubs.onlinelibrary.wiley.com/doi/pdf/10.1029/2025JC022530, 2025.

Nielsdóttir, M. C., Bibby, T. S., Moore, C. M., Hinz, D. J., Sanders, R., Whitehouse, M., Korb, R., and Achterberg, E. P.: Seasonal and spatial dynamics of iron availability in the Scotia Sea, Marine Chemistry, 130-131, 62–72, https://doi.org/10.1016/j.marchem.2011.12.004, 2012.

Nędzarek, A.: Sources, diversity and circulation of biogenic compounds in Admiralty Bay, King George Island, Antarctica, Antarctic Science, 20, 135–145, https://doi.org/10.1017/S0954102007000909, 2008.

Oetjens, A.: Data for the physical transport processes in the fjords of South Georgia - Polarstern PS133-2 Island Impact, https://zenodo.org/records/18981814?preview=1&token=eyJhbGciOiJIUzUxMiJ9.eyJpZCI6ImJmZjU3MmY5LWI4MWUtNDM1ZC1iYTczLWFhMWRmNDM1NmRhOSIsImRhdGEiOnt9LCJyYW5kb20iOiI5NTU\protect\penalty\z@xMDVmNTUzMzNiMWYwOTliODM0MDgwMDA2Njc0MCJ9.8bm4a6E5Xwpew39FGrguwKcrwIOOQC4JsYtR4\protect\penalty\z@SEZj5WGYA__loY-VNk-ASwQL_8RDmetZMheP7QRU3VjGMu2FA, 2025.

Orsi, A. H., Whitworth, T., and Nowlin, W. D.: On the meridional extent and fronts of the Antarctic Circumpolar Current, Deep Sea Research Part I: Oceanographic Research Papers, 42, 641–673, https://doi.org/10.1016/0967-0637(95)00021-W, 1995.

https://doi.org/10.5194/egusphere-2026-1808
Preprint. Discussion started: 10 April 2026

Park, Y., Park, T., Kim, T., Lee, S., Hong, C., Lee, J., Rio, M., Pujol, M., Ballarotta, M., Durand, I., and Provost, C.: Observations of the Antarctic Circumpolar Current Over the Udintsev Fracture Zone, the Narrowest Choke Point in the Southern Ocean, Journal of Geophysical Research: Oceans, 124, 4511–4528, https://doi.org/10.1029/2019JC015024, 2019.

Pfeffer, W. T.: A simple mechanism for irreversible tidewater glacier retreat, Journal of Geophysical Research, 112, F03S25, https://doi.org/10.1029/2006JF000590, 2007.

Pollard, R., Sanders, R., Lucas, M., and Statham, P.: The Crozet Natural Iron Bloom and Export Experiment (CROZEX), Deep Sea Research Part II: Topical Studies in Oceanography, 54, 1905–1914, https://doi.org/10.1016/j.dsr2.2007.07.023, 2007.

Raiswell, R., Benning, L. G., Davidson, L., and Tranter, M.: Nanoparticulate bioavailable iron minerals in icebergs and glaciers, Mineralogical Magazine, 72, 345–348, https://doi.org/10.1180/minmag.2008.072.1.345, 2008.

Raven, J. A.: The iron and molybdenum use efficiencies of plant growth with different energy, carbon and nitrogen sources, New Phytologist, 109, https://doi.org/10.1111/j.1469-8137.1988.tb04196.x, 1988.

Robinson, J., Popova, E. E., Srokosz, M. A., and Yool, A.: A tale of three islands: Downstream natural iron fertilization in the Southern Ocean, Journal of Geophysical Research: Oceans, 121, 3350–3371, https://doi.org/10.1002/2015JC011319, 2016.

Stimpfle, J., Koch, F., Ebner, B., Völkner, C., Zitoun, R., Sukekava, C. F., Sander, S. G., Henkel, S., Bundy, R. M., Ruacho, A., Kasten, S., and Trimborn, S.: Glacially derived iron is more bioavailable to Antarctic phytoplankton than other sources, Communications Earth & Environment, 7, 89, https://doi.org/10.1038/s43247-025-03092-5, publisher: Nature Publishing Group, 2026.

Tichit, P., Brickle, P., Newton, R. J., Convey, P., and Dawson, W.: Introduced species infiltrate recent stages of succession after glacial retreat on sub-Antarctic South Georgia, NeoBiota, 92, 85–110, https://doi.org/10.3897/neobiota.92.117226, 2024.

Tippenhauer, S., Klaas, C., and Kasten, S.: Raw data of physical oceanography during RV POLARSTERN cruises PS133/1 and PS133/2, https://doi.org/10.1594/PANGAEA.962314, type: dataset, 2023.

Varela, D. E. and Harrison, P. J.: Effect of ammonium on nitrate utilization by Emiliania huxleyi, a coccolithophore from the oceanic northeastern Pacific, Marine Ecology Progress Series, 186, 67–74, https://www.jstor.org/stable/24853293, publisher: Inter-Research Science Center, 1999.

Wadham, J. L., De'ath, R., Monteiro, F. M., Tranter, M., Ridgwell, A., Raiswell, R., and Tulaczyk, S.: The potential role of the Antarctic Ice Sheet in global biogeochemical cycles, Earth and Environmental Science Transactions of the Royal Society of Edinburgh, 104, 55–67, https://doi.org/10.1017/S1755691013000108, 2013.

Ward, P., Whitehouse, M., Shreeve, R., Thorpe, S., Atkinson, A., Korb, R., Pond, D., and Young, E.: Plankton community structure south and west of South Georgia (Southern Ocean): Links with production and physical forcing, Deep Sea Research Part I: Oceanographic Research Papers, 54, 1871–1889, https://doi.org/10.1016/j.dsr.2007.08.008, 2007.

Wehrmann, L. M., Formolo, M. J., Owens, J. D., Raiswell, R., Ferdelman, T. G., Riedinger, N., and Lyons, T. W.: Iron and manganese speciation and cycling in glacially influenced high-latitude fjord sediments (West Spitsbergen, Svalbard): Evidence for a benthic recycling-transport mechanism, Geochimica et Cosmochimica Acta, 141, 628–655, https://doi.org/10.1016/j.gca.2014.06.007, 2014.

Whitehouse, M., Priddle, J., and Symon, C.: Seasonal and annual change in seawater temperature, salinity, nutrient and chlorophyll a distributions around South Georgia, South Atlantic, Deep Sea Research Part I: Oceanographic Research Papers, 43, 425–443, https://doi.org/10.1016/0967-0637(96)00020-9, 1996.

Whitney, F. A. and Freeland, H. J.: Variability in upper-ocean water properties in the NE Pacific Ocean, Deep Sea Research Part II: Topical Studies in Oceanography, 46, 2351–2370, https://doi.org/10.1016/S0967-0645(99)00067-3, 1999.

https://doi.org/10.5194/egusphere-2026-1808
Preprint. Discussion started: 10 April 2026

Young, E., Rock, J., Meredith, M., Belchier, M., Murphy, E., and Carvalho, G.: Physical and behavioural influences on larval fish retention: contrasting patterns in two Antarctic fishes, Marine Ecology Progress Series, 465, 201–215, https://doi.org/10.3354/meps09908, 2012.

Young, E. F., Meredith, M. P., Murphy, E. J., and Carvalho, G. R.: High-resolution modelling of the shelf and open ocean adjacent to South Georgia, Southern Ocean, Deep Sea Research Part II: Topical Studies in Oceanography, 58, 1540–1552, https://doi.org/10.1016/j.dsr2.2009.11.003, 2011.

Young, E. F., Thorpe, S. E., Banglawala, N., and Murphy, E. J.: Variability in transport pathways on and around the South Georgia shelf, Southern Ocean: Implications for recruitment and retention, Journal of Geophysical Research: Oceans, 119, 241–252, https://doi.org/10.1002/2013JC009348, 2014.

Zanker, J. C., Young, E., Holland, P. R., Haigh, I. D., and Brickle, P.: Oceanographic Variability in Cumberland Bay, South Georgia, and Its Implications for Glacier Retreat, Journal of Geophysical Research: Oceans, 129, e2023JC020 507, https://doi.org/10.1029/2023JC020507, _eprint: https://agupubs.onlinelibrary.wiley.com/doi/pdf/10.1029/2023JC020507, 2024.